THE EUROPEAN
PHYSICAL JOURNAL C

Regular Article - Theoretical Physics

Nucleon strangeness polarization from $\Lambda/\bar{\Lambda}$ hyperon production in polarized proton–proton collision at RHIC

Xiaonan Liu[1], Bo-Qiang Ma[1,2,3,a]

[1] School of Physics and State Key Laboratory of Nuclear Physics and Technology, Peking University, Beijing 100871, China
[2] Collaborative Innovation Center of Quantum Matter, Beijing, China
[3] Center for High Energy Physics, Peking University, Beijing 100871, China

Abstract We calculate the inclusive production of a polarized Λ or $\bar{\Lambda}$ hyperon from the single longitudinally polarized proton and proton (pp) collision at RHIC. By comparing the data reported by the STAR Collaboration, we find that this process is sensitive to the polarization of strange and antistrange quarks of the proton in the experimental range. By introducing asymmetric coefficients with the minimization of χ^2, we further identify the asymmetry of the polarized strange–antistrange quarks in the proton sea and find that the first moment is $\Delta s \approx -0.025 \pm 0.019$ for strange quark and $\Delta\bar{s} \approx -0.001 \pm 0.012$ for antistrange quark, with central values agreeing with the light-cone meson–baryon fluctuation model prediction, the recent lattice QCD determination of strangeness polarization and results from a global QCD analysis given by the Jefferson Lab Angular Momentum (JAM) Collaboration.

1 Introduction

The spin content of the proton has received extensive attentions since the so-called "proton spin crisis" [1,2]. There have been significant progress on spin distributions of light flavor valence quarks both experimentally and theoretically. Recently, some efforts have been made on the polarization of the light flavor sea quarks [3,4] and the quark–antiquark asymmetry of helicity distributions in nucleon sea [5]. Studies of the momentum distribution asymmetry between strange and antistrange [6–10] are of significance for the study of nonperturbative quantum chromodynamics (QCD) with fruitful progress [11–29]. However, the understanding of helicity distributions for strange–antistrange quark pairs $\Delta s(x)$ and $\Delta\bar{s}(x)$ is far from satisfactory and needs further studies. Researches show that studies of spin-transfer

reactions [30–42] and measurements of the polarized structure function [1,2,43–48], can provide new insights into the nucleon spin structure and yield a better understanding of the hadronization process. The Λ baryon plays a special role in this respect since it has a rather simple spin structure in the naive quark parton model [49], as well as that its self-analyzing parity violating decays [50] make polarization measurements experimentally feasible.

The STAR experiment at Relativistic Heavy Ion Collider (RHIC) [51–53] is carrying out a spin physics program in high-energy polarized proton–proton collisions at $\sqrt{s} = 200$ GeV and $\sqrt{s} = 500$ GeV in order to gain a deeper insight into the nucleon spin structure and dynamics of the proton. Theoretical investigations [33,35,36,38–42] suggest that the spin transfer process of the $\Lambda/\bar{\Lambda}$ production in the singly polarized proton–proton collision provides a platform to extract polarized parton distribution functions of the proton and polarized quark fragmentation functions of quarks into $\Lambda/\bar{\Lambda}$ hyperon. The experiments measuring the polarization of Λ hyperon produced in singly polarized pp collisions [54,55] may provide information about not only the inclusive production of hadrons but also the strange and antistrange quark polarizations inside the proton.

Compared to lepton-induced reaction experiments, the corresponding cross section of the hadron–hadron collision is larger and the luminosity of the incoming proton beams can be made higher. Moreover, there are many subprocesses that may lead to the final state Λ in singly polarized pp collisions due to the rich internal structure of the proton, such as $qq \rightarrow qq$, $qg \rightarrow qg$, $gg \rightarrow gg$, etc., which may produce large partonic spin asymmetries. Therefore productions of Λ and $\bar{\Lambda}$ are sensitive to polarized parton distributions in the proton, making STAR ideal to explore quark and gluon polarization.

In this work, we perform the calculation of longitudinal spin transfers to Λ and $\bar{\Lambda}$ hyperons produced in polar-

[a] e-mail: mabq@pku.edu.cn

ized proton–proton collisions at RHIC. By comparing recent data [55] reported by the STAR Collaboration, we find that this process is sensitive to the polarization of strange and anti-strange quarks of the proton in the experimental range. Such result agrees with the conclusions in previous studies [40–42]. By introducing asymmetric coefficients with the minimization of χ^2 in fitting data, we further identify the asymmetry of the polarized strange–antistrange quarks in the proton and find that the first moment is $\Delta s \approx -0.025 \pm 0.019$ for strange quark and $\Delta\bar{s} \approx -0.001 \pm 0.012$ for antistrange quark, with central values agreeing with the light-cone meson–baryon fluctuation model prediction [6], the recent lattice QCD determination of strangeness polarization [56] and results from a global QCD analysis given by the Jefferson Lab Angular Momentum (JAM) Collaboration [57].

The reminder of this paper is organized as follows. Sect. 2.1 provides general formulae for production cross section. As the $\Lambda/\bar{\Lambda}$ hyperon production process in singly polarized pp collisions contains many different hard subprocesses, Sect. 2.2 elucidates kinematic regions and identifies the major subprocess. We then calculate fragmentation functions for quarks to Λ in Sect. 2.3. Numerical results of the spin transfer to $\Lambda/\bar{\Lambda}$ are shown in Sect. 3.1 with considerations of the asymmetry of polarized strange–antistrange quarks in the proton, together with discussions and conclusions. A brief summary is given in Sect. 4.

2 Theoretical calculation

2.1 The general formulae for cross section

We consider the single inclusive production process $\vec{p}\, p \to \vec{\Lambda}\, X$, where a polarized $\Lambda/\bar{\Lambda}$ is produced from the single longitudinally polarized pp collision at RHIC. The longitudinal spin transfer to $\Lambda/\bar{\Lambda}$ hyperon produced in polarized proton–proton collisions is defined as [30]

$$A^{\Lambda/\bar{\Lambda}} = E\frac{d^3\Delta\sigma}{d^3 p} \Big/ E\frac{d^3\sigma}{d^3 p},$$

where $d\Delta\sigma$ and $d\sigma$ stand for the polarized and unpolarized cross sections, respectively. The definition and derivation of the parton–parton scattering contribution to the single-particle inclusive cross section can be found in Refs. [58,59]. By using factorization theorem [60], the differential cross-section for high-transverse momentum distributions has been computed to next-to-leading order accuracy in perturbative QCD [61–63]. In this way, such cross sections can be expressed as convolutions of perturbatively calculable partonic spin-transfer cross sections [30,31,35] with certain sets of parton distributions and fragmentation functions at the

scale Q, just as follows,

$$
\begin{aligned}
&E\frac{d^3\Delta\sigma}{d^3 p}(\text{AB} \to \text{C} + \text{X}) \\
&= \sum_{abcd} \int_{\bar{x}_a}^1 dx_a \int_{\bar{x}_b}^1 dx_b \Delta f_a^{\text{A}}(x_a, Q^2) \\
&\quad f_b^{\text{B}}(x_b, Q^2) \Delta D_c^{\text{C}}(z_c, Q^2)\frac{1}{\pi z_c} \\
&\quad \frac{d\Delta\hat{\sigma}}{d\hat{t}}(ab \to cd),
\end{aligned}
\tag{1}
$$

with

$$
\begin{aligned}
z_c &= \frac{x_{\text{T}}}{2x_b}e^{-\eta} + \frac{x_{\text{T}}}{2x_a}e^{\eta}, \\
\bar{x}_b &= \frac{x_a x_{\text{T}} e^{-\eta}}{2x_a - x_{\text{T}}e^{\eta}}, \\
\bar{x}_a &= \frac{x_{\text{T}} e^{\eta}}{2 - x_{\text{T}}e^{-\eta}},
\end{aligned}
\tag{2}
$$

here η and p_{T} are rapidity and transverse momentum, and $x_{\text{T}} = 2p_{\text{T}}/\sqrt{s}$ is the transverse momentum counterpart. We denote the momenta of incoming protons and the produced hyperon by P_{A}, P_{B} and P_{C}, respectively. x_a, x_b and z_c are corresponding momentum fractions carried by partons a, b and c, and $\bar{x}_a$ and $\bar{x}_b$ are corresponding lower limits of integration.

In Eq. (1), $\Delta f_a^{\text{A}}(x_a, Q^2)$ represents the polarized distribution function of parton a in proton A and $f_b^{\text{B}}(x_b, Q^2)$ the unpolarized one of parton b in proton B, at the scale Q. $\Delta D_c^{\text{C}}(z_c, Q^2)$ is the polarized fragmentation function of parton c into baryon C, and in our case $\text{C} = \Lambda$. $\Delta d\hat{\sigma}/d\hat{t}$, the difference of cross sections at the parton level between the two processes $a^\uparrow + b \to c^\uparrow + d$ and $a^\downarrow + b \to c^\uparrow + d$, can be found in, for example, Ref. [30]. The summation in Eq. (1) runs over all possible parton–parton subprocesses, $qq \to qq$, $qg \to qg$, $q\bar{q} \to q\bar{q}$, etc. An analogous expression for unpolarized cross section is obtained by Eq. (1) with the Δ symbol dropped throughout. In the calculation we adopt de Florian–Sassot–Stratmann–Vogelsang (DSSV) polarized parton distribution functions (PDFs) [64,65] as inputs to spin-dependent parton distributions of proton A directly. With sufficient statistics, this set of PDFs not only provides the total up and down quarks distributions, $\Delta u + \Delta\bar{u}$ and $\Delta d + \Delta\bar{d}$, and light sea quark polarizations, $\Delta\bar{u}$, $\Delta\bar{d}$, $\Delta\bar{s} = \Delta s$, but also gives an important constraint on the gluon polarization Δg. Considering that this set of PDFs adopts Martin–Stirling–Thorne–Watt (MSTW) unpolarized PDFs [66] as a reference set to avoid problems with the fundamental positivity constraint, we adopt the MSTW parametrization as unpolarized PDFs for proton B in order to maintain self-consistency. The non-perturbative fragmentation functions for Λ are given by the revised Gribov–

Lipatov relation [67–71] and the light-cone SU(6) quark–spectator–diquark model [72,73] adjusted by the Albino–Kniehl–Kramer (AKK) parametrization [74,75] based on considerations following Ref. [29].

The Mandelstam variables at the parton level are given by

$$\hat{s} = x_a x_b s,$$
$$\hat{t} = -x_a p_T \sqrt{s} e^{-\eta}/z_c, \qquad (3)$$
$$\hat{u} = -x_b p_T \sqrt{s} e^{\eta}/z_c,$$

here s is the total center of mass energy.

It is obvious from Eq. (2) that the lower limits of momentum fraction of the initial state, $\bar{x}_a$ and $\bar{x}_b$, depend mainly on experimental conditions, namely rapidity η and transverse momentum p_T. The momentum fraction carried by the final state baryon, z_c, is also related to the momentum fraction of the initial state. Note that the magnitude of momentum fractions represents different regions of momentum distributions, that is, the region where the momentum fraction is smaller is mainly the sea region, and the region where the momentum fraction is larger is the valence region. Such general relationships can help us to analyze the dynamic range of pp collisions in the calculation and to obtain an understanding of the spin transfer in this process.

2.2 Elucidate the kinematic regions and major subprocess

The main aim of the spin transfer process to $\Lambda/\bar{\Lambda}$ hyperon produced in pp collisions is to extract the polarized quark and gluon distributions. However, in the case of pp collisions where many subprocesses can lead to final state hyperons, we need to identify out the most contributing channel related to the polarized parton distributions.

We first check the relation between $\bar{x}_a$, the integral lower limit of x_a, and p_T using Eq. (2). The small value of p_T is associated with x_a in the sea part of the polarized proton whereas typical values of x_a corresponding to the valence region correspond to a high p_T, where the quarks are polarized much more strongly, resulting in an asymmetry increase with p_T. Information about contribution from parton distributions of the polarized proton can also be tracked from looking at the x_a dependence of η. Similarly, if there is a large positive η, this can be used to extract the large x_a part parton content of the proton. The high p_T and large η lead to dominating contribution to the spin transfer to final state hyperons with the valence part of the polarized proton. Hence it is reasonably to conclude that in large p_T region in pp collisions, the fragmentation of quarks from the subprocesses $qg \rightarrow qg$ and $qq \rightarrow qq$ dominates. We expect that u and d, particularly u, quark fragmentation dominates the Λ production in high p_T and large rapidity region, as supported by previous studies [33,35,36,38]. The connection between x_b and x_a

allows us to further determine the dynamic behavior. It can be seen from Eq. (2) that when x_a is small, x_b is relatively large and mainly corresponds to the valence region, and as x_a increases, the integral lower limit of x_b gradually expands to the sea region. Considering that the gluon is distributing much greater over the sea region of the proton than quarks, the sum of valence and sea quark contributions is suppressed at small x_a and x_b. It means that the subprocess $qg \rightarrow qg$ plays a major role than $qq \rightarrow qq$ case [35,36]. It is also argued in Ref. [35] that the contribution from $gg \rightarrow gg$ falls off faster than that from $qg \rightarrow qg$ with increasing rapidity, since $g(x_a)$ decreases faster than $q(x_a)$ with increasing x_a. Therefore we can conclude that the $qg \rightarrow qg$ subprocess plays the most important role in the $\Lambda/\bar{\Lambda}$ hyperon production of proton–proton collisions [33,35,36,38], so we only consider the spin transfer of this subprocess.

Based on the above considerations, the process of our calculation can be expressed as:

$$[\Delta q^p(x_a) g^p(x_b) + \Delta g^p(x_a) q^p(x_b)]$$
$$\rightarrow [\Delta D_q^\Lambda(z_c) + \Delta D_g^\Lambda(z_c)]. \qquad (4)$$

Specifically, this contains four subprocesses:

(1) $\Delta q^{p_A} g^{p_B} \rightarrow \Delta q^\Lambda g$;
(2) $\Delta q^{p_A} g^{p_B} \rightarrow \Delta g^\Lambda q$;
(3) $\Delta g^{p_A} q^{p_B} \rightarrow \Delta q^\Lambda g$;
(4) $\Delta g^{p_A} q^{p_B} \rightarrow \Delta g^\Lambda q$.

We write the detailed expressions in the following way:

$$\Delta q^{p_A}(x_a) g^{p_B}(x_b)$$
$$\frac{d\sigma}{dt}(\hat{t}, \hat{u})[\Delta D_q^\Lambda(z_c) + T^{\vec{q} g \rightarrow q \vec{g}}(y) \Delta D_g^\Lambda(z_c)],$$
$$\Delta g^{p_A}(x_a) q^{p_B}(x_b) \qquad (5)$$
$$\frac{d\sigma}{dt}(\hat{u}, \hat{t})[T^{q \vec{g} \rightarrow \vec{q} g}(y) \Delta D_q^\Lambda(z_c) + \Delta D_g^\Lambda(z_c)],$$

where $q = u, d, s$, with $T^{\vec{q} g \rightarrow \vec{q} g}(y) = 1$ omitted and $T^{q \vec{g} \rightarrow \vec{q} g}(y) = T^{\vec{q} g \rightarrow q \vec{g}}(y) = (1 - (1 - y)^2)/(1 + (1 - y)^2)$ being the polarization transfer factor for the two subprocesses, see Ref. [38] for details. Due to that the fragmentation mechanism of the polarized gluon into Λ is unclear, we take $\Delta D_g^\Lambda = 0$ in our calculation. Likewise, we use corresponding expressions analogy to Eq. (5) for the longitudinal spin transfer to $\bar{\Lambda}$, by replacing q with $\bar{q}$. There are several differences in the calculation of $\bar{\Lambda}$ compared to Λ. For $\bar{\Lambda}$ hyperon, the dominant subprocess should be $\Delta \bar{q} g \rightarrow \Delta \bar{q} g$, where we take $\Delta D_{\bar{q}}^{\bar{\Lambda}} = \Delta D_q^\Lambda$ according to CP symmetry. Due to the lack of fragmentation functions for polarized sea quarks to Λ, we set $\Delta D_q^{\bar{\Lambda}} = \Delta D_{\bar{q}}^\Lambda = 0$ in the calculation, based on same considerations as the gluon case. Different from the Λ
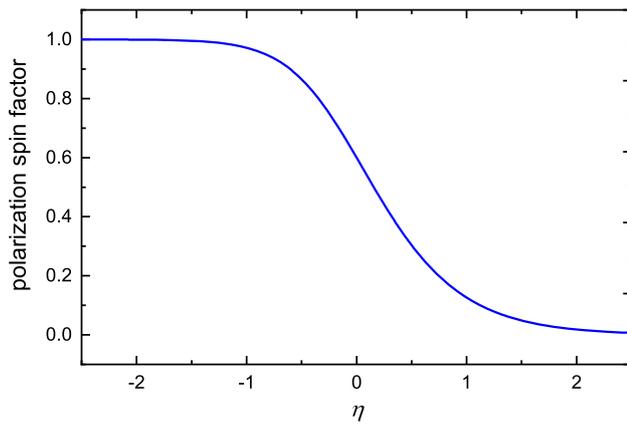
Fig. 1 The polarization transfer factor $T(\eta)$ versus rapidity η of the process $qg \to qg$. The solid curve represents the longitudinal polarization transfer factor of the process $\Delta g \to \Delta q$. The polarization transfer factor for $T^{\Delta q \to \Delta q}(\eta) = 1$ is not presented in the picture

case, the polarized sea quarks play a main role in the process of spin transfer to $\bar{\Lambda}$, in which distributions of polarized sea quarks are relatively important.

For hadron–hadron collisions, each of the parton subprocess has its own polarization transfer factor. For the polarization transfer factor $T(y)$, the variable $y = p_B \cdot (p_A - p_C)/(p_A \cdot p_B)$, and in the center-of-mass frame $y = (1 - \cos(\theta))/2$, where $\theta = 2 \arctan(\exp(-\eta))$ is the angle between the incoming parton a and the outgoing parton c. Figure 1 shows the polarization transfer factor $T(\eta)$ versus rapidity η of the process $qg \to qg$. It can be seen that for the process $q\overrightarrow{g} \to \overrightarrow{q}g$ the longitudinal polarization transfer factor $T^{q\overrightarrow{g} \to \overrightarrow{q}g}(\eta)$ gradually tends to zero, as rapidity increases. There is no dependence on rapidity for the longitudinal process $\overrightarrow{q}g \to \overrightarrow{q}g$ with $T^{\overrightarrow{q}g \to \overrightarrow{q}g}(\eta) = 1$.

2.3 Fragmentation functions and AKK parametrization

Fragmentation functions (FFs) describe phenomena of hadronization, i.e., how quarks or gluons transform into hadrons. The improvement in the knowledge of fragmentation functions is an important ingredient in the global analysis of the nucleon spin structure. PDFs and FFs cannot be computed perturbatively, but they can be measured from a limited set of data over a limited range of Q. Because it is easier to extract PDFs from experiment than FFs, it would be very useful if there exists simple connection [69–71] between PDFs and FFs, so that one can predict the poorly known $D_q(z)$ from the rather well known $q(x)$. We adopt a revised form of the Gribov-Lipatov "reciprocity" relation [67–71], i.e.,

$$D(z) \propto zq(z), \tag{6}$$

to obtained fragmentation functions for Λ, with PDFs described by the SU(6) quark–diquark model [72,73].

Gribov and Lipatov [67,68] provided a connection between distinct physical situations in deep inelastic electron scattering in perturbation theory. Brodsky and Ma [69] have shown that the fragmentation functions $D_q^H(z, Q^2)$ measured in quark and jet hadronization at $z \simeq 1$ are related by crossing to the quark distributions $q(x, Q^2)$ measured in deep inelastic scattering processes at $x \simeq 1$, a limit with both sides in physical regions is also proved by Barone et al. [70]. Ma et al. [71] further studied the relation between the quark distribution function $q(x, Q^2)$ and the fragmentation function $D_q^H(z, Q^2)$. Their work supports the revised Gribov–Lipatov relation $D(z) = zq(z)$ at $z \to 1$, as an approximate relation for the connection between distribution and fragmentation functions. In fact, most other theoretical estimates [32,76–79] on the quark fragmentation functions are also based on some knowledge of quark distributions. Note that such a relation provides successful descriptions of the available Λ polarization data in several processes [25,29,36,73,80], despite the crudeness of the model and the limited range of the Gribov–Lipatov reciprocity relation, we still expect that the above estimate can serve as a reasonable guide to the size of the expected effects.

As an explanation to understand proton spin puzzle [81, 82], one can construct the light-cone SU(6) quark–spectator–diquark model of the proton [83,84] by taking into account the relativistic effect of the quark transversal motions, i.e., the Melosh–Wigner rotation effect [85–88], to calculate the valence quark spin distributions in the light-cone formalism, which provides a convenient framework for the relativistic description of hadrons in terms of quark degree of freedom. The Melosh–Wigner rotation is one of the most important ingredients of the light-cone formalism, and it helps to built up the quark helicity distributions of the nucleon [83,84].

The light-cone SU(6) quark–spectator–diquark model can be extended from the nucleon to the Λ hyperon [72,73]. The unpolarized valence quark distributions $u_v(x), d_v(x)$ and $s_v(x)$ for Λ are given in this model by

$$
\begin{aligned}
d_v^\Lambda(x) &= u_v^\Lambda(x) \\
&= \frac{1}{4}a_V(x) + \frac{1}{12}a_S(x), \\
s_v^\Lambda(x) &= \frac{1}{3}a_S(x),
\end{aligned}
\tag{7}
$$

where $a_D(x)$ ($D = S$ for scalar spectator or V for axial vector spectator) denotes the amplitude for quark q to be scattered while the spectator is in the diquark state $D(qq)$. To obtain an estimate of $a_D(x)$, we employ the Brodsky-Huang-Lepage (BHL) prescription [89,90] of the light-cone momentum space wave function

$$\varphi_D(x, \mathbf{k}_\perp)$$
$$= A_D \exp\left\{ -\frac{1}{8}\alpha_D^2 \left[\frac{(m_q^2 + \mathbf{k}_\perp^2)}{x} + \frac{(m_D^2 + \mathbf{k}_\perp^2)}{(1-x)} \right] \right\}$$

with parameters (in units of MeV) $\alpha_D = 330$, and $m_q = 330$, $m_{S(ud)} = 750$, $m_{V(ud)} = 950$ for $q = u$ and d, $m_q = 480$, $m_{S(s)} = 600$, $m_{V(s)} = 800$ for $q = s$ [72,73]. When expressed in terms of the light-cone momentum space wave function $\varphi_D(x, \mathbf{k}_\perp)$, $a_D(x)$ reads $a_D(x) \propto \int [d^2\mathbf{k}_\perp] \, | \varphi_D(x, \mathbf{k}_\perp) |^2$ and is normalized such that $\int_0^1 dx\, a_D(x) = 3$.

The quark helicity distributions for $u_v(x)$, $d_v(x)$ and $s_v(x)$ quarks for Λ can be written as

$$\Delta d_v^\Lambda(x) = \Delta u_v^\Lambda(x)$$
$$= -\frac{1}{12}a_V(x)M_q^V(x) + \frac{1}{12}a_S(x)M_q^S(x), \quad (8)$$
$$\Delta s_v^\Lambda(x) = \frac{1}{3}a_S(x)M_q^S(x),$$

in which $M_q^S(x)$ and $M_q^V(x)$ are Melosh–Wigner correction factors for scalar and axial vector spectator–diquark cases. They are obtained by averaging $M_q^D(x, \mathbf{k}_\perp) = ((k^+ + m)^2 - \mathbf{k}_\perp^2)/((k^+ + m)^2 + \mathbf{k}_\perp^2)$ over $\mathbf{k}_\perp$ with $k^+ = x\mathcal{M}$ and $\mathcal{M}^2 = (m_q^2 + \mathbf{k}_\perp^2)/x + (m_D^2 + \mathbf{k}_\perp^2)/(1-x)$, where m_D is the mass of the diquark spectator. From Eq. (7) we get $a_S(x) = 3s_v^\Lambda(x)$, $a_V(x) = 4u_v^\Lambda(x) - s_v^\Lambda(x)$ and then have

$$\Delta d_v^\Lambda(x) = \Delta u_v^\Lambda(x)$$
$$= \frac{1}{4}s_v^\Lambda(x)M_q^S(x) - \frac{1}{12}(4u_v^\Lambda(x) - s_v^\Lambda(x))M_q^V(x),$$
$$\Delta s_v^\Lambda(x) = s_v^\Lambda(x)M_q^S(x). \quad (9)$$

Thus we arrive at simple relations between the polarized and unpolarized quark distributions for the valence $u_v(x)$, $d_v(x)$ and $s_v(x)$ quarks.

According to Eqs. (6–9), we obtain not only the unpolarized but also the polarized fragmentation functions of valence quarks of Λ with parton distribution functions and helicity distributions calculated by the SU(6) quark–spectator–diquark model [72,73]. The helicity distributions for valence quarks of Λ calculated by the SU(6) quark–diquark model, are shown in Fig. 2 (the solid curves), with the distributions for u_v and d_v quarks being identical.

In order to reproduce the experimental data in a reasonable form, we adjust the fragmentation functions obtained by theoretical calculations with AKK parametrization [75] as an input. The sea quark distribution functions for the proton can take the parametrization directly, with the other octet baryons such as Λ obtained from the SU(3) symmetry [91]. Considering that AKK FFs for Λ production are defined to be sum of those for Λ and $\bar{\Lambda}$, and according to
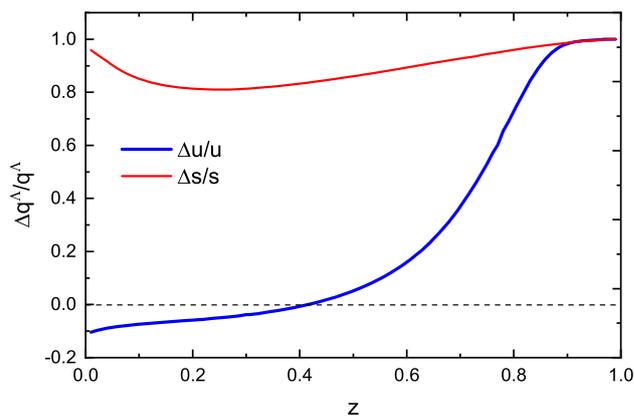

Fig. 2 The helicity distributions for valence quarks of Λ obtained by SU(6) quark–diquark model [72,73], in which distributions for u_v and d_v quarks are identical. The thick solid curve and the thin solid curve represent the helicity distributions of u_v and s_v quarks, respectively

$D_q^{\Lambda+\bar{\Lambda}} = D_{q+\bar{q}}^\Lambda = D_{q+\bar{q}}^{\bar{\Lambda}}$, we modify the fragmentation functions obtained by the light-cone model as Ref. [29]:

$$D_q^\Lambda(z, Q^2) = \left(\frac{D_q^\Lambda(z)}{D_{q+\bar{q}}^\Lambda(z)} \right)^{th} D_{q+\bar{q}}^\Lambda(z, Q^2)^{AKK},$$
$$D_{\bar{q}}^\Lambda(z, Q^2) = \left(\frac{D_{\bar{q}}^\Lambda(z)}{D_{q+\bar{q}}^\Lambda(z)} \right)^{th} D_{q+\bar{q}}^\Lambda(z, Q^2)^{AKK}, \quad (10)$$
$$\Delta D_q^\Lambda(z, Q^2) = \left(\frac{\Delta D_q^\Lambda(z)}{D_{q+\bar{q}}^\Lambda(z)} \right)^{th} D_{q+\bar{q}}^\Lambda(z, Q^2)^{AKK},$$

where $q = u, d, s$.

Considering that the light-cone model does not provide information on gluon fragmentation, we take $D_g^\Lambda(z, Q^2) = D_g^\Lambda(z, Q^2)^{AKK}$ directly. So far, there is no clear understanding of the polarized fragmentation function of the gluon into Λ. For simplicity, but without loss of generality, we may take $\Delta D_g^\Lambda(z, Q^2) = 0$ in our calculation at first. In Sect. 3.2, we consider $\Delta D_g^\Lambda(z, Q^2) = D_g^\Lambda(z, Q^2)(\Delta g^\Lambda(z, Q^2)/g^\Lambda(z, Q^2))$ by assuming that the gluon polarization behaves in a similar way between the octet baryons. The two cases may assess how big is the impact of neglecting $\Delta D_g^\Lambda(z, Q^2)$. In this way of parametrization, the unpolarized sea distributions and gluon distributions may be included as those of the input parametrization, thus the sea part and the valence part of quark distributions are consistent with each other. The fragmentation functions are also reasonably scale dependent as they are mainly based on the parametrization set. Therefore we construct a set of polarized fragmentation functions for quark to Λ in consistent with available parametrization of unpolarized fragmentation functions, with additional separation between quark and antiquark fragmentation functions [29].
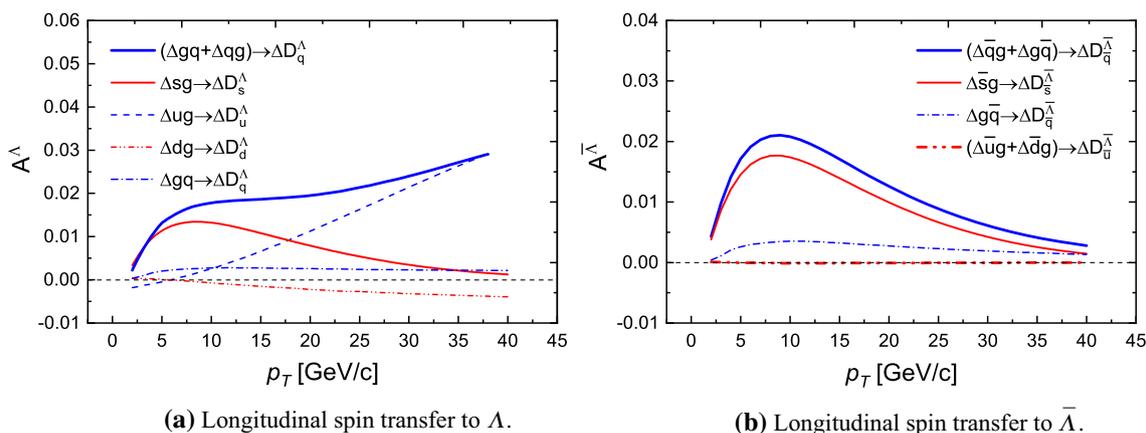
(a) Longitudinal spin transfer to Λ.

(b) Longitudinal spin transfer to $\bar{\Lambda}$.

Fig. 3 The calculated spin transfers to Λ and $\bar{\Lambda}$ of quarks and gluon for positive η versus p_{T} at $\sqrt{s} = 200$ GeV. The thick solid curves represent the total contributions from the polarized quarks/antiquarks and gluon, and the thin solid curves represent the spin transfer of the s quark for the channel $\Delta sg \rightarrow \Delta D_s^\Lambda$. The channels for the polarized u (the dashed curves) and d (the dashed dot dot curves) quarks, and g (the dashed dot curves) are also shown in the plots

3 Results

3.1 The symmetric case for $\Delta s = \Delta \bar{s}$

We calculate the spin transfer of the inclusive production process of a polarized $\Lambda/\bar{\Lambda}$ from single longitudinally polarized $\vec{p}\,p$ collision under the $qg \rightarrow qg$ subprocess at $\sqrt{s} = 200$ GeV. The final results for the spin transfer to $\Lambda/\bar{\Lambda}$ with integration over $\eta \in (0, 1.2)$ and renormalization scale $Q = p_{\mathrm{T}}$ are presented in Fig. 3. A conventional range of variation is $p_{\mathrm{T}}/2 < Q < 2p_{\mathrm{T}}$. In this work, the hard scale, Q, is set equal to the transverse momentum p_{T}. According to Refs. [33,35], for instance, there is only a very weak dependence on the scale by calculating the polarization using $Q = p_{\mathrm{T}}/2$ and $Q = 2p_{\mathrm{T}}$. We show various contributions from the polarized quarks/antiquarks and gluon in Fig. 3a for Λ and Fig. 3b for $\bar{\Lambda}$ and also their total contributions (the thick solid curves). Clearly, the difference between Λ and $\bar{\Lambda}$ is significant for the total spin transfer, whereas the contributions from the polarized strange–antistrange quarks, where we take $\Delta s(x) = \Delta \bar{s}(x)$ from the DSSV set of the proton polarized PDFs [64,65], are similar for Λ and $\bar{\Lambda}$ cases. The spin transfers of the s quark (the thin solid curves) for the channel $\Delta s \rightarrow \Delta D_s^\Lambda$, become large around $p_{\mathrm{T}} \sim 5$–10 GeV and gradually decrease with p_{T} increasing. Note that channels for the polarized u quarks (the dashed curves), including also d quarks (the dashed dot dot curves), contribute significantly in large p_{T} region, thus it is reasonable to conclude that the difference mainly comes from the valence part of quarks between Λ and $\bar{\Lambda}$, due to the zero contribution from valence quark to $\bar{\Lambda}$ fragmentation because of $\Delta D_q^{\bar{\Lambda}} = 0$ in our calculation. In addition, in spite of the suppression from polarization transfer factor $T^{q\vec{g} \rightarrow \vec{q}g}$ (see the solid curve in Fig. 1), we also find a sizeable contribution due to the gluon

polarization (the dashed dot curves) transferred to the quark polarization in the longitudinal spin transfers to Λ and $\bar{\Lambda}$ in Fig. 3b. This indicates that the measurement of the spin transfer to Λ and particularly $\bar{\Lambda}$ may provide additional information concerning the gluon polarization.

We compare the calculated results, as shown in Fig. 4 with the dashed curves, with experimental data [55] reported by the STAR Collaboration. The STAR Collaboration extracted the longitudinal spin transfers to Λ and $\bar{\Lambda}$ hyperons in $\sqrt{s} = 200$ GeV polarized proton–proton collisions for extended p_{T} up to 7 GeV/c with mid-rapidity $|\eta| < 1.2$ covered during the 2009 RHIC run. Figure 4 reveals that our calculated results can reasonably fit the data points within err-bars.

3.2 The asymmetric case for $\Delta s \neq \Delta \bar{s}$

Since the spin transfer of strange quark to $\Lambda/\bar{\Lambda}$ dominates within the experimental range, based on previous analysis, it is interesting to further explore the effect on the behaviour of strangeness. This may provide more information about the polarized strange quark in the proton through the spin transfer process. The strange quark distribution in the nucleon is usually obtained from analyses of the deep inelastic lepton-nucleon scattering data by assuming identical momentum distribution for the strange and antistrange quark distributions, i.e., $s(x) = \bar{s}(x)$. According to Refs. [6–10], however, the distributions of sea quarks and antiquarks, which are intrinsic to the nucleon bound state wave function, need not be identical.

To investigate the contribution to the spin transfer difference between Λ and $\bar{\Lambda}$ hyperons from the nucleon asymmetric strange–antistrange sea distribution, we need an asymmetric strange sea input. The light-cone meson–baryon fluctuation model [6], where the nucleon wave function at low
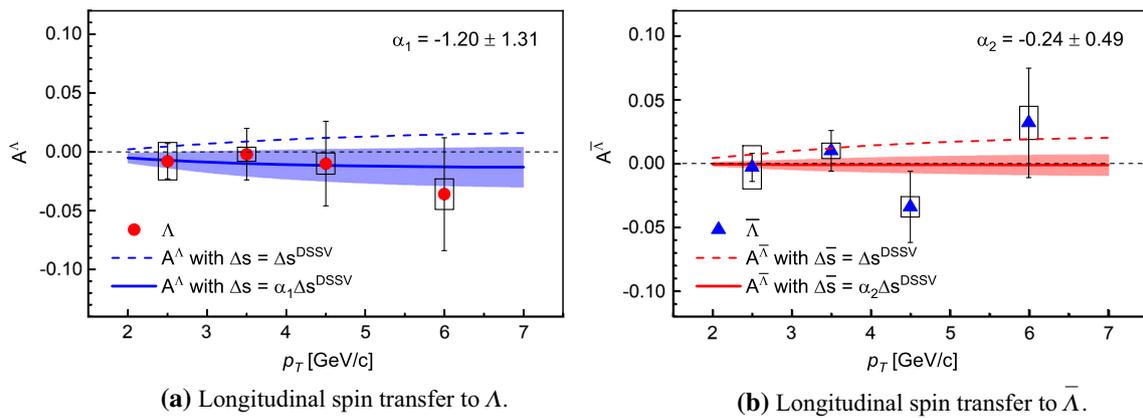
(a) Longitudinal spin transfer to Λ.

(b) Longitudinal spin transfer to $\bar{\Lambda}$.
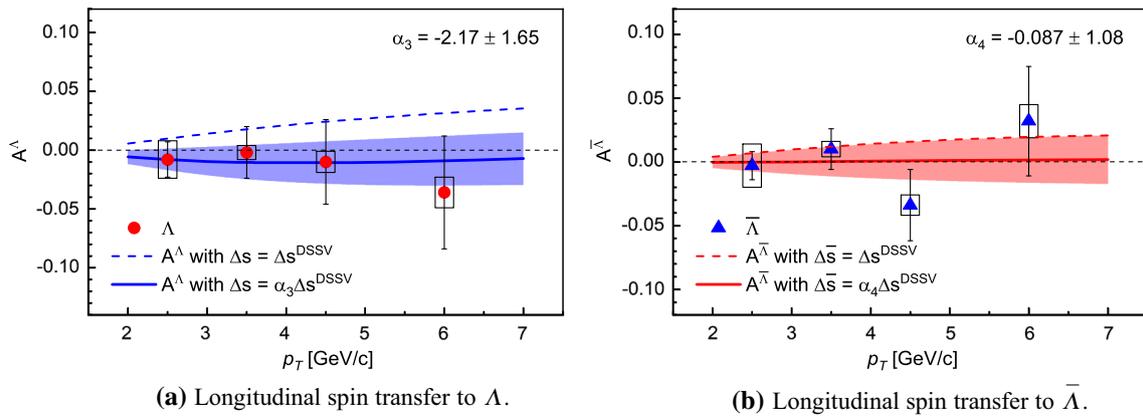
Fig. 4 Comparison of the measured spin transfer data with theory predictions A^{Λ} and $A^{\bar{\Lambda}}$ for positive η versus p_T at $\sqrt{s} = 200$ GeV. Markers with error bars are the data collected by the STAR Collaboration [55]. The vertical bars and boxes indicate the sizes of the statistical and systematical uncertainties, respectively. The solid curve represents the result with the asymmetric input of the polarized strange and antistrange quarks, and the dashed curve, with cuts to a much smaller range in p_T compared to Fig. 3, represents the result with the symmetric input of the polarized strange and antistrange quarks. The asymmetric coefficients α_i for corresponding process are presented with errors. The shadow region covers the error band. More details about the fitting results of α_i are presented in Table 1

Table 1 Fitting results of α_i and calculated results of Δs and $\Delta \bar{s}$

Coefficient	Value	Δs	$\Delta \bar{s}$	$\chi^2_{\min}$
α_1	-1.20 ± 1.31	-0.014 ± 0.015		0.37
α_2	-0.24 ± 0.49		-0.003 ± 0.005	2.48

resolution can be viewed as a fluctuating system coupling to the intermediate baryon–meson Fock state $p(uuds\bar{s}) = \Lambda(uds) + K^+(u\bar{s})$, predicts the nucleon asymmetric strange–antistrange sea distributions: the intrinsic s quarks in the proton sea are negatively polarized, whereas the intrinsic s antiquarks give zero contributions to the proton spin. From previous results, we see that under the present experimental conditions, the spin transfer process from proton to Λ is sensitive to the polarized strange and antistrange quarks. The results in Fig. 4 also illustrate this point well. In order to further explore the influence of the polarized strange and antistrange quarks, a strange–antistrange asymmetry is given in the following way.

To test the asymmetry of the polarized strange–antistrange quarks in the proton, based on the assumption $\Delta s(x) = \Delta \bar{s}(x)$ provided by the DSSV parametrization [64,65], we take an asymmetric coefficient on the polarized strange quark with $\Delta s^{\text{th}} = \alpha_1 \Delta s^{\text{DSSV}}$, and antistrange quark with $\Delta \bar{s}^{\text{th}} = \alpha_2 \Delta \bar{s}^{\text{DSSV}}$, respectively. To insure that the value of the asymmetric coefficients α_i are in a reasonable physical range, we adopt the relation $|\Delta s^{\text{th}}| = |\alpha_i \Delta s^{\text{DSSV}}| \leq s^{\text{MSTW}}$ to satisfy the constraint condition in energy scale $p_T < 7$ GeV. By making a χ^2 test with the simplest form $\chi^2 = \sum_n (A_n^{\Lambda,\text{th}} - A_n^{\Lambda,\text{data}})^2 / \sigma_n^2$ on the value of α_i between range $(\alpha_{i,\min}, \alpha_{i,\max})$, we obtain the fitting results of α_i with corresponding $\chi^2_{\min}$ and errors in Table 1. We also calculate the first moment of the modified polarized strange quark,

$\int_{\bar{x}_a}^1 dx \Delta s(x, Q^2)^{\text{th}} = \alpha_1 \int_{\bar{x}_a}^1 dx \Delta s(x, Q^2)^{\text{DSSV}}$, and the corresponding antiquark counterpart $\int_{\bar{x}_a}^1 dx \Delta \bar{s}(x, Q^2)^{\text{th}} = \alpha_2 \int_{\bar{x}_a}^1 dx \Delta \bar{s}(x, Q^2)^{\text{DSSV}}$. We then compare the calculated results with the light-cone meson–baryon fluctuation model prediction. According to the calculated results presented in Table 1, where the first moment is $\Delta s \approx -0.014 \pm 0.015$ for strange quark and $\Delta \bar{s} \approx -0.003 \pm 0.005$ for antistrange quark, we see that the central values of the fitting results are basically consistent with the model prediction $\Delta s \approx -0.05$ to -0.01 and $\Delta \bar{s} \approx 0$.

We also compare our results of spin transfers A^{Λ} and $A^{\bar{\Lambda}}$ with the experiment data in Fig. 4, with the solid curves representing the results with the asymmetric input of the polarized strange and antistrange quarks. The asymmetric coefficients α_i for corresponding processes are presented with errors. The shadow region covers the error band. One can see that the spin transfer to $\Lambda/\bar{\Lambda}$ in the polarized pp collision is sensitive to the polarization of strange–antistrange quarks and the fitting results can describe the experimental data within a reasonable error range.

Since the polarization of gluon is not negligible, it is unreasonable to take $\Delta D_g^{\Lambda}(z, Q^2) = 0$ in an oversimplified and crude way. As before, due to the lack of the knowledge of the polarized gluon fragmentation into Λ, it makes sense to consider $\Delta D_g^{\Lambda}(z, Q^2) = D_g^{\Lambda}(z, Q^2)(\Delta g^{\Lambda}(z, Q^2)/g^{\Lambda}(z, Q^2))$ assuming that the gluon polarization behaves in a similar way between the octet baryons, i.e.,

Table 2 Fitting results of α_i and calculated results of Δs and $\Delta \bar{s}$

Coefficient	Value	Δs	$\Delta \bar{s}$	$\chi^2_{\min}$
α_3	-2.17 ± 1.65	-0.025 ± 0.019		0.42
α_4	-0.087 ± 1.08		-0.001 ± 0.012	2.24

(a) Longitudinal spin transfer to Λ.

(b) Longitudinal spin transfer to $\bar{\Lambda}$.

Fig. 5 Comparison of the measured spin transfer data with theory predictions A^Λ and $A^{\bar{\Lambda}}$ for positive η versus p_T at $\sqrt{s} = 200$ GeV, including the contribution from the polarized gluon fragmentation. The symbols and curves are identical with Fig. 4. More details about the fitting results of α_i are presented in Table 2
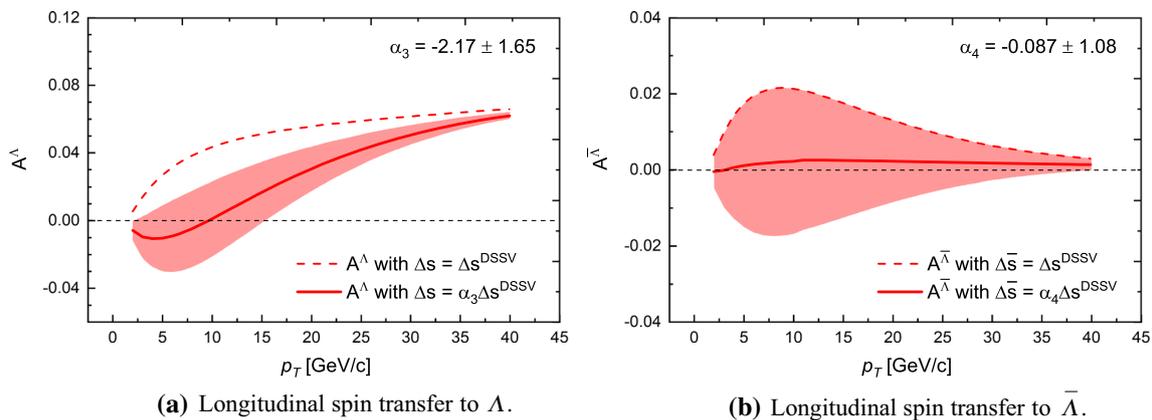

(a) Longitudinal spin transfer to Λ.

(b) Longitudinal spin transfer to $\bar{\Lambda}$.

Fig. 6 The calculated spin transfers A^Λ and $A^{\bar{\Lambda}}$ for positive η versus p_T at $\sqrt{s} = 200$ GeV, including the contribution from the polarized gluon fragmentation. The solid curve represents the result with the asymmetric input of the polarized strange and antistrange quarks, and the dashed curve represents the result with the symmetric input of the polarized strange and antistrange quarks. The asymmetric coefficients α_i for corresponding process are presented with errors. The shadow region covers the error band

$$\Delta g^\Lambda(z, Q^2)/g^\Lambda(z, Q^2) = \Delta g^p(z, Q^2)/g^p(z, Q^2).$$

As already remarked, we take the spin-dependent parton distribution functions for the proton from DSSV set [64,65], the spin-averaged parton distribution functions for the proton from MSTW set [66], and the unpolarized fragmentation functions for Λ from AKK set [74,75], respectively.

We compute also the longitudinal spin transfer to $\Lambda/\bar{\Lambda}$ including the fragmentation from polarized gluon, and find that the cross section for pp collisions is sensitive to the ΔD_g^Λ contribution owing to a large, positive gluon polariza-

tion of the proton. In the following, we denote α_3 and α_4 as the asymmetric coefficients, and present the calculated results in Table 2 and compare in Fig. 5 the results with data. As one can see, it is worth mentioning that the asymmetry between the strange/antistrange quark is enhanced in this case, with the first moment is $\Delta s \approx -0.025 \pm 0.019$ for strange quark and $\Delta \bar{s} \approx -0.001 \pm 0.012$ for antistrange quark. It is interesting to notice that the central value of our new results $\Delta s^+ = \Delta s + \Delta \bar{s} = -0.026 \pm 0.022$ agrees with the recent lattice QCD determination of strangeness polarization, $\Delta s^+ = -0.02 \pm 0.01$ at $Q^2 \approx 7$ GeV^2 [56], and a more

negative value, $\Delta s^+ = -0.03 \pm 0.10$, given by the Jefferson Lab Angular Momentum (JAM) Collaboration [57].

We finally compare in Fig. 6 the results for the symmetric and asymmetric cases of polarized strange–antistrange quarks, including the contribution from the polarized gluon fragmentation. The solid curve represents the result with the asymmetric input of the polarized strange and antistrange quarks, and the dashed curve represents the result with the symmetric input of the polarized strange and antistrange quarks. We note that there is significant difference between asymmetric and symmetric cases, thus further improvement of the precision in experiments can distinguish the two cases to shed light on the strange–antistrange polarization asymmetry of the nucleon sea.

4 Summary

In summary, we study the inclusive production process of polarized $\Lambda/\bar{\Lambda}$ from a single longitudinally polarized pp collision at $\sqrt{s} = 200$ GeV. Based on the analysis of kinematic regions, the $qg \rightarrow qg$ subprocess plays a major role in proton–proton collision processes. By comparing calculated results with data reported by the STAR Collaboration [55], we find that this process is sensitive to the polarization of strange and antistrange quarks within the experimental range $\eta \in (0, 1.2)$ and $p_T < 7$ GeV. By introducing asymmetric coefficients with the minimization of χ^2, we further identify the asymmetry of the polarized strange–antistrange quarks in protons. We find that the first moment is $\Delta s \approx -0.025 \pm 0.019$ for strange quark and $\Delta \bar{s} \approx -0.001 \pm 0.012$ for antistrange quark, which agrees with the light-cone meson–baryon fluctuation model prediction [6], the recent lattice QCD determination of strangeness polarization [56] and results from a global QCD analysis given by the Jefferson Lab Angular Momentum (JAM) Collaboration [57]. The significant difference between symmetric and asymmetric cases suggests that the spin transfer process of $\vec{p} p \rightarrow \vec{\Lambda} X$ is feasible to study strange–antistrange polarizations. The large statistical errors of data are also the reason why fitting errors are large, and high precision experiments are expected to shed light on the strangeness spin structure of the nucleon.

Data Availability Statement This manuscript has associated data in a data repository. [Authors' comment: The experimental data used in the present study have been published by the STAR Collaboration [55].]

References

1. J. Ashman et al., [European Muon Collaboration], Phys. Lett. B **206**, 364 (1988)
2. J. Ashman et al., [European Muon Collaboration], Nucl. Phys. B **328**, 1 (1989)
3. F. Tian, C. Gong, B.-Q. Ma, Nucl. Phys. A **961**, 154 (2017)
4. F. Tian, C. Gong, B.-Q. Ma, Nucl. Phys. A **968**, 379 (2017)
5. M. Liu, B.-Q. Ma, Phys. Rev. D **98**(3), 036024 (2018)
6. S.J. Brodsky, B.-Q. Ma, Phys. Lett. B **381**, 317 (1996)
7. A.I. Signal, A.W. Thomas, Phys. Lett. B **191**, 205 (1987)
8. M. Burkardt, B. Warr, Phys. Rev. D **45**, 958 (1992)
9. H. Holtmann, A. Szczurek, J. Speth, Nucl. Phys. A **596**, 631 (1996)
10. R.S. Sufian, T. Liu, G.F. de Tramond, H.G. Dosch, S.J. Brodsky, A. Deur, M.T. Islam, B.-Q. Ma, Phys. Rev. D **98**, 114004 (2018)
11. B.-Q. Ma, Phys. Lett. B **408**, 387 (1997)
12. V. Barone, C. Pascaud, F. Zomer, Eur. Phys. J. C **12**, 243 (2000)
13. Y. Ding, B.-Q. Ma, Phys. Lett. B **590**, 216 (2004)
14. Y. Ding, R.G. Xu, B.-Q. Ma, Phys. Lett. B **607**, 101 (2005)
15. M. Wakamatsu, Phys. Rev. D **71**, 057504 (2005)
16. J. Alwall, G. Ingelman, Phys. Rev. D **71**, 094015 (2005)
17. Y. Ding, R.G. Xu, B.-Q. Ma, Phys. Rev. D **71**, 094014 (2005)
18. P. Gao, B.-Q. Ma, Eur. Phys. J. C **44**, 63 (2005)
19. G. Hao, L. Li, C.F. Qiao, Phys. Lett. B **621**, 139 (2005)
20. C. Bourrely, J. Soffer, F. Buccella, Phys. Lett. B **648**, 39 (2007)
21. M. Diehl, T. Feldmann, P. Kroll, Phys. Rev. D **77**, 033006 (2008)
22. P. Gao, B.-Q. Ma, Eur. Phys. J. C **50**, 603 (2007)
23. P. Gao, B.-Q. Ma, Phys. Rev. D **77**, 054002 (2008)
24. S.S. Zhou, Y. Chen, Z.T. Liang, Q.H. Xu, Phys. Rev. D **79**, 094018 (2009)
25. Y. Chi, X. Du, B.-Q. Ma, Phys. Rev. D **90**(7), 074003 (2014)
26. T.J. Hobbs, M. Alberg, G.A. Miller, Phys. Rev. C **91**, 035205 (2015)
27. M. Wakamatsu, Phys. Rev. D **90**(3), 034005 (2014)
28. A. Vega, I. Schmidt, T. Gutsche, V.E. Lyubovitskij, Phys. Rev. D **93**, 056001 (2016)
29. X. Du, B.-Q. Ma, Phys. Rev. D **95**(1), 014029 (2017)
30. J.F. Owens, Rev. Mod. Phys. **59**, 465 (1987)
31. M. Stratmann, W. Vogelsang, Phys. Lett. B **295**, 277 (1992)
32. A. Kotzinian, A. Bravar, D. von Harrach, Eur. Phys. J. C **2**, 329 (1998)
33. D. de Florian, M. Stratmann, W. Vogelsang, Phys. Rev. Lett. **81**, 530 (1998)
34. B.-Q. Ma, I. Schmidt, J. Soffer, J.J. Yang, Eur. Phys. J. C **16**, 657 (2000)
35. C. Boros, J.T. Londergan, A.W. Thomas, Phys. Rev. D **62**, 014021 (2000)
36. B.-Q. Ma, I. Schmidt, J. Soffer, J.J. Yang, Nucl. Phys. A **703**, 346 (2002)
37. J.R. Ellis, A. Kotzinian, D.V. Naumov, Eur. Phys. J. C **25**, 603 (2002)
38. Q.H. Xu, C.X. Liu, Z.T. Liang, Phys. Rev. D **65**, 114008 (2002)
39. Q.H. Xu, Z.T. Liang, Phys. Rev. D **70**, 034015 (2004)
40. Q.H. Xu, Z.T. Liang, E. Sichtermann, Phys. Rev. D **73**, 077503 (2006)
41. Y. Chen, Z.T. Liang, E. Sichtermann, Q.H. Xu, S.S. Zhou, Phys. Rev. D **78**, 054007 (2008)
42. W. Zhou, S.S. Zhou, Q.H. Xu, Phys. Rev. D **81**, 057501 (2010)
43. D. Adams et al., [Spin Muon (SMC) Collaboration], Phys. Lett. B **329**, 399 (1994)
44. K. Abe et al., [E143 Collaboration]. Phys. Rev. Lett. **74**, 346 (1995)

45. K. Abe et al., [E154 Collaboration]. Phys. Rev. Lett. **79**, 26 (1997)
46. D. Adams et al., [Spin Muon (SMC) Collaboration]. Phys. Rev. D **56**, 5330 (1997)
47. B. Adeva et al., [Spin Muon Collaboration]. Phys. Rev. D **58**, 112001 (1998)
48. A. Airapetian et al., [HERMES Collaboration]. Phys. Rev. D **75**, 012007 (2007)
49. M. Gell-Mann, Phys. Lett. **8**, 214 (1964)
50. T.D. Lee, C.N. Yang, Phys. Rev. **108**, 1645 (1957)
51. M. Harrison, S.G. Peggs, T. Roser, Ann. Rev. Nucl. Part. Sci. **52**, 425 (2002)
52. M. Harrison, T. Ludlam, S. Ozaki, Nucl. Instrum. Methods A **499**, 235 (2003)
53. E.D. Courant, Ann. Rev. Nucl. Part. Sci. **53**, 1 (2003)
54. B.I. Abelev et al., [STAR Collaboration]. Phys. Rev. D **80**, 111102 (2009)
55. J. Adam et al., [STAR Collaboration], Phys. Rev. D **98**(11), 112009 (2018)
56. G.S. Bali et al., [QCDSF Collaboration]. Phys. Rev. Lett. **108**, 222001 (2012)
57. J.J. Ethier, N. Sato, W. Melnitchouk, Phys. Rev. Lett. **119**(13), 132001 (2017)
58. S.M. Berman, J.D. Bjorken, J.B. Kogut, Phys. Rev. D **4**, 3388 (1971)
59. S.D. Ellis, M.B. Kislinger, Phys. Rev. D **9**, 2027 (1974)
60. J.C. Collins, D.E. Soper, Ann. Rev. Nucl. Part. Sci. **37**, 383 (1987)
61. F. Aversa, P. Chiappetta, M. Greco, J.P. Guillet, Nucl. Phys. B **327**, 105 (1989)
62. D. de Florian, Phys. Rev. D **67**, 054004 (2003)
63. B. Jager, A. Schafer, M. Stratmann, W. Vogelsang, Phys. Rev. D **67**, 054005 (2003)
64. D. de Florian, R. Sassot, M. Stratmann, W. Vogelsang, Phys. Rev. Lett. **101**, 072001 (2008)
65. D. de Florian, R. Sassot, M. Stratmann, W. Vogelsang, Phys. Rev. D **80**, 034030 (2009)
66. A.D. Martin, W.J. Stirling, R.S. Thorne, G. Watt, Eur. Phys. J. C **63**, 189 (2009)
67. V.N. Gribov, L.N. Lipatov, Phys. Lett. **37B**, 78 (1971)
68. V.N. Gribov, L.N. Lipatov, Sov. J. Nucl. Phys. **15**, 438 (1972)
69. S.J. Brodsky, B.-Q. Ma, Phys. Lett. B **392**, 452 (1997)
70. V. Barone, A. Drago, B.-Q. Ma, Phys. Rev. C **62**, 062201 (2000)
71. B.-Q. Ma, I. Schmidt, J. Soffer, J.J. Yang, Phys. Lett. B **547**, 245 (2002)
72. B.-Q. Ma, I. Schmidt, J.J. Yang, Phys. Lett. B **477**, 107 (2000)
73. B.-Q. Ma, I. Schmidt, J.J. Yang, Phys. Rev. D **61**, 034017 (2000)
74. S. Albino, B.A. Kniehl, G. Kramer, Nucl. Phys. B **734**, 50 (2006)
75. S. Albino, B.A. Kniehl, G. Kramer, Nucl. Phys. B **803**, 42 (2008)
76. M. Burkardt, R.L. Jaffe, Phys. Rev. Lett. **70**, 2537 (1993)
77. D. Ashery, H.J. Lipkin, Phys. Lett. B **469**, 263 (1999)
78. M. Anselmino, M. Boglione, F. Murgia, Phys. Lett. B **481**, 253 (2000)
79. C.X. Liu, Z.T. Liang, Phys. Rev. D **62**, 094001 (2000)
80. B.-Q. Ma, I. Schmidt, J. Soffer, J.J. Yang, Phys. Rev. D **62**, 114009 (2000)
81. B.-Q. Ma, J. Phys. G **17**, L53 (1991)
82. B.-Q. Ma, Q.-R. Zhang, Z. Phys. C **58**, 479 (1993)
83. B.-Q. Ma, Phys. Lett. B **375**, 320 (1996)
84. B.-Q. Ma, I. Schmidt, J. Soffer, Phys. Lett. B **441**, 461 (1998)
85. E.P. Wigner, Ann. Math. **40**, 149 (1939)
86. E.P. Wigner, Nucl. Phys. Proc. Suppl. **6**, 9 (1989)
87. H.J. Melosh, Phys. Rev. D **9**, 1095 (1974)
88. F. Buccella, C.A. Savoy, P. Sorba, Lett. Nuovo Cim. **10**, 455 (1974)
89. S.J. Brodsky, T. Huang, G.P. Lepage, Conf. Proc. C **810816**, 143 (1981)
90. T. Huang, B.-Q. Ma, Q.X. Shen, Phys. Rev. D **49**, 1490 (1994)
91. B.-Q. Ma, I. Schmidt, J. Soffer, J.J. Yang, Phys. Rev. D **65**, 034004 (2002)